

KRAP is required for diffuse and punctate IP₃-mediated Ca²⁺ liberation and determines the number of functional IP₃R channels within clusters

Irene Vorontsova^a, Jeffrey T. Lock^a, Ian Parker^{a,b,*}

^a Department of Neurobiology & Behavior, UC Irvine, Irvine, CA, United States

^b Department of Physiology & Biophysics, UC Irvine, Irvine, CA, United States

ARTICLE INFO

Keywords:

KRAP
IP₃ receptor
Calcium puffs
Calcium fluctuation imaging
Calcium waves

ABSTRACT

KRAS-induced actin-interacting protein (KRAP) has been identified as crucial for the appropriate localization and functioning of the inositol trisphosphate receptors (IP₃Rs) that mediate Ca²⁺ release from the endoplasmic reticulum. Here, we used siRNA knockdown of KRAP expression in HeLa and HEK293 cells to examine the roles of KRAP in the generation of IP₃-mediated local Ca²⁺ puffs and global, cell-wide Ca²⁺ signals. High resolution Ca²⁺ imaging revealed that the mean amplitude of puffs was strongly reduced by KRAP knockdown, whereas the Ca²⁺ flux during openings of individual IP₃R channels was little affected. In both control and KRAP knockdown cells the numbers of functional channels in the clusters underlying puff sites were stochastically distributed following a Poisson relationship, but the mean number of functional channels per site was reduced by about two thirds by KRAP knockdown. We conclude that KRAP is required for activity of IP₃R channels at puff sites and stochastically ‘licenses’ the function of individual channels on a one-to-one basis, rather than determining the functioning of the puff site as a whole. In addition to puff activity (‘punctate’ Ca²⁺ release), global, cell-wide Ca²⁺ signals evoked by higher levels of IP₃ are further composed from a discrete ‘diffuse’ mode of Ca²⁺ release. By applying fluctuation analysis to isolate the punctate component during global Ca²⁺ signals, we find that KRAP knockdown suppresses to similar extents punctate and diffuse Ca²⁺ release in wild-type cells and in HEK293 cells exclusively expressing type 1 and type 3 IP₃Rs. Thus, KRAP appears essential for the functioning of the IP₃Rs involved in diffuse Ca²⁺ release as well as the clustered IP₃Rs that generate local Ca²⁺ puffs.

1. Introduction

A major cellular signaling pathway involves the liberation of Ca²⁺ ions sequestered in the endoplasmic reticulum (ER) into the cytosol through inositol 1,4,5-trisphosphate receptors (IP₃Rs) in the ER membrane [1]. Opening of the intrinsic channel formed by these tetrameric receptors is regulated by both IP₃ and by cytosolic Ca²⁺ [2–4]. The latter feature endows a regenerative property of Ca²⁺-induced Ca²⁺ release (CICR), so that in the presence of IP₃, Ca²⁺ released through an open channel may trigger the opening of adjacent IP₃R channels. The patterning of Ca²⁺ signals is further defined by the spatial distribution of IP₃Rs across the ER. Whereas most IP₃Rs within the ER membrane are motile, a small fraction (~30%) are grouped in immotile clusters that contain a few to a few tens of IP₃Rs [5,6] and are predominantly located near the plasma membrane [6,7]. The concerted openings of channels within these clusters generate local cytosolic Ca²⁺ transients (Ca²⁺ puffs) that typically last tens of milliseconds and are restricted to within

~2 μm [7]. Puffs are preferentially activated at low levels of IP₃, and appear as a flurry of activity during the initial rising phase of global, cell-wide Ca²⁺ signals evoked by higher levels of IP₃ [8–13]. Because puffs are a ubiquitous feature of Ca²⁺ signaling in many cell types there is much interest in determining how the underlying IP₃Rs are assembled into clusters, how these become anchored at fixed sites, and how they are ‘licensed’ to preferentially respond at low [IP₃].

Several reports implicate KRAS-induced actin-interacting protein (KRAP; also known as sperm-specific antigen 2 (SSFA2); and as IP₃ receptor interacting domain-containing protein 2 (ITPRID 2) [14]) as a potential key molecular player for both the spatial organization and functional activity of IP₃Rs [15–17]. Notably, Thillaiappan et al. [17] described that KRAP tethered IP₃Rs to actin filaments close beneath the plasma membrane where puff sites are located, and reported that knockdown of KRAP by siRNA abolished both Ca²⁺ puffs and the global increases in cytosolic Ca²⁺ concentration evoked by higher levels of IP₃. Conversely, over-expressing KRAP resulted in immobilization of additional IP₃R clusters, an increase in numbers of Ca²⁺ puffs, and larger

* Corresponding author.

E-mail address: iparker@uci.edu (I. Parker).

<https://doi.org/10.1016/j.ceca.2022.102638>

Received 13 May 2022; Received in revised form 3 August 2022; Accepted 11 August 2022

Available online 19 August 2022

0143-4160/© 2022 The Authors. Published by Elsevier Ltd. This is an open access article under the CC BY license (<http://creativecommons.org/licenses/by/4.0/>).

Abbreviations

CICR	Ca ²⁺ -induced Ca ²⁺ release
ER	endoplasmic reticulum
IP ₃	inositol trisphosphate
IP ₃ R	inositol trisphosphate receptor
KRAP	K-Ras-induced actin-interacting protein
TIRF	total internal reflection fluorescence
ROI	region of interest
siRNA	small interfering RNA

global Ca²⁺ signals. KRAP thus appears to be crucial for anchoring and functionally licensing the clustered IP₃Rs that generate local puffs and being obligatory for global Ca²⁺ signals evoked by higher levels of IP₃.

These two roles would be easily reconciled in the context of a widely held model wherein global, cell-wide Ca²⁺ responses are generated by the coordinated activation of local puffs by successive cycles of Ca²⁺ release, diffusion and CICR as the Ca²⁺ wave propagates across IP₃R clusters [8,9,12,17–23]. If puffs were thus the fundamental building block from which all cellular Ca²⁺ signals are generated, then their disruption by the absence of KRAP would readily explain the attenuation of global Ca²⁺ spikes. However, interpretation is complicated by recent findings that local puff activity ('punctate' Ca²⁺ liberation) largely terminates about mid-way during the rise of global Ca²⁺ spikes, and that the greater fraction of the total Ca²⁺ release originates through a distinct, 'diffuse' mode of Ca²⁺ liberation [10,11].

Thillaiappan et al. [17] further observed that overexpression of KRAP increased the frequency of puffs and the number of sites at which they occurred, without affecting the mean amplitude of puffs. Conversely, KRAP knockdown massively reduced the number of observed puff sites, almost completely abolishing IP₃-evoked puffs. From these findings they concluded that the level of KRAP expression determines the number of immobile IP₃R puncta, suggesting an intriguing mechanism whereby KRAP captures pre-existing IP₃R clusters, tethers them to actin and licenses these clusters to respond to IP₃ in a 'binary', all-or-none manner. That is to say, the 'quantal unit' licensed by KRAP is a preestablished cluster of IP₃Rs, rather than individual IP₃Rs within a cluster.

Prompted by these findings, we investigated two aspects of the role of KRAP in regulating Ca²⁺ release through IP₃Rs. (i) Does the expression level of KRAP differentially affect the punctate and diffuse modes of Ca²⁺ release? (ii) Does KRAP license individual IP₃R channels to enable them to flux Ca²⁺ when activated by IP₃, or are entire IP₃R clusters licensed as a functional unit? To experimentally address these questions, we applied fluctuation analysis of Ca²⁺ fluorescence signals [10,11,24] as a sensitive measure of both global puff activity and the activity of individual IP₃R channels.

2. Materials and methods

2.1. Cell culture

Experiments were performed using HeLa cells (ATCC #CCL-2), and HEK293 cells genetically engineered to exclusively express either IP₃R1 or IP₃R3 (Kerafast #EUR031 and #EUR033). Cells were cultured in Eagle's Minimum Essential Medium (EMEM; ATCC #30–2003) supplemented with 10% fetal bovine serum (Omega Scientific #FB-11) in plastic t25 or t75 cm² flasks and were maintained at 37 °C in a humidified incubator gassed with 95% air and 5% CO₂.

2.2. siRNA knockdown

siRNA-targeting KRAP (#M-015,325–01–0005), non-targeting

control siRNA (#D-001,206–13–05), and siGLO red transfection indicator (#D-001,630–02–05) were purchased from Dharmacon (Chicago, IL) and prepared as 20 μM stock solutions according to the manufacturer's instructions; all were stored at –20 °C until use. The siRNA targeting KRAP was a 'SMARTpool' combination of four gene-specific siRNAs, specified by the manufacturer to improve the likelihood of effective gene silencing and minimize sequence-specific off-targeting by lowering the relative concentration of each siRNA. For transfection, HeLa or HEK293 cells were collected using 0.25% Trypsin-EDTA (ThermoFisher #25,200–056) and grown on 60 mm culture dishes. When cells were 80% confluent, they were incubated with either 24 nM KRAP siRNA ('KRAP knockdown cells') or 24 nM control siRNA ('control cells') together with DharmaFect transfection reagent (Cat #: T-2001–02) in OPTI-MEM (ThermoFisher; Cat #: 31,985,062) for 4–6 hrs. In all transfections, cells were additionally incubated with 2.4 nM siGLO Red transfection indicator to serve as a fluorescent tracer to visualize transfection efficiency and as a fiducial marker for selecting cells during imaging experiments. Following transfection, cells were harvested using 0.25% Trypsin-EDTA, resuspended in EMEM, and plated on 35 mm glass-bottom imaging dishes (MatTek #P35–1.5–14-C; Ashland, MA) where they were grown for 48 hrs prior to imaging. To improve adhesion of HEK293 cells these were plated on poly-D-lysine (Millipore Sigma #P0899; St. Louis, MO) coated (1 mg/ml) imaging dishes. For both KRAP knockdown and control groups, those cells showing strong uptake of the SiGLO Red transfection indicator were selected for imaging.

2.3. Cell loading

Cells were incubated with 5 μM of the membrane-permeant fluorescent Ca²⁺ indicator Cal520-AM (AAT Bioquest #21,130; Sunnyvale, CA) for 1 hr at room temperature in a Ca²⁺-containing HEPES buffered salt solution (Ca²⁺-HBSS) together with 5 μM of the membrane-permeant ester of the caged IP₃ analogue ci-IP₃-PM (D-2,3,-O-Isopropylidene-6-O-(2-nitro-4,5 dimethoxy) benzyl-myoinositol 1,4,5,-triphosphate hexakis (propionoxymethyl) ester) (SiChem #cagiso2-145–10; Bremen, Germany). In some experiments cells were additionally loaded by incubation with EGTA-AM (15 μM; Thermo Fisher Scientific #E1219) for a further 1 hr at room temperature in Ca²⁺-HBSS. Following loading, cells were maintained for 30 min at room temperature in Ca²⁺-HBSS before imaging. Cal520-AM, ci-IP₃-PM, and EGTA-AM were all solubilized with DMSO/20% pluronic F127 (ThermoFisher #P3000MP). Ca²⁺-HBSS contained (in mM) 135 NaCl, 5.4 KCl, 2 CaCl₂, 1 MgCl₂, 10 HEPES, and 10 glucose (pH=7.4). Zero Ca²⁺-HBSS consisted of the same formulation with CaCl₂ omitted, and 300 μM EGTA added. The receptor agonists carbachol (#C4832) and histamine (#H7125) were purchased from Millipore Sigma and solubilized in zero Ca²⁺-HBSS.

2.4. Imaging

Total internal reflection fluorescence (TIRF) imaging of Ca²⁺ signals was accomplished using two microscope systems. All data, except Fig. 1 and supplemental Figs. S1 and S2, were acquired using a Nikon Eclipse microscope system (Nikon, Melville, NY, USA) with a 100X (NA 1.49) TIRF oil objective. Fluorescence of Cal520 was excited by 488-nm laser light, and emitted fluorescence (λ>510 nm) was imaged at 120 frames per second using an electron-multiplied CCD Camera (iXon DU897; Andor, Belfast, UK). Image data were acquired at 16 bit depth, using 2 × 2 binning for a final field at the specimen of 130 × 130 binned pixels (one binned pixel = 0.32 μm) and were stored as stack.nd2 files using Nikon Elements for offline analysis. A flash of ultraviolet (UV) light (350–400 nm) from an arc lamp was focused to uniformly illuminate a region slightly larger than the imaging field to photorelease i-IP₃. The amount of i-IP₃ released was controlled by varying the flash duration with an electronically controlled shutter and neutral density filters.

Data in Fig. 1 and supplemental Figs. S1 and S2 were acquired using

a home-built microscope system [7] based around an Olympus (Center Valley, PA) IX50 microscope equipped with an Olympus 60X oil immersion TIRF objective (NA 1.45) and an Evolve EMCCD camera (Photometrics; Tucson, AZ) with a bit depth of 16 bits, using 2×2 binning for a final field at the specimen of 128×128 binned pixels (one binned pixel = $0.53 \mu\text{m}$) at a rate of 125 frames per second. Image data were streamed to computer memory using Metamorph v7.7 (Molecular Devices; San Jose, CA) and stored on hard disk for offline analysis. Cal520 fluorescence was excited using a 488 nm laser and detected through a 510 nm long-pass (LP) emission filter. Receptor agonists were locally applied through glass micropipettes (tip diameters 1–2 μm) positioned above the cell, using a pneumatic picospritzer. Agonist delivery was empirically adjusted to evoke rapid rises in whole-cell cytosolic Ca^{2+} levels in control cells.

All imaging was performed at room temperature, with cells bathed in zero Ca^{2+} -HBSS. All cytosolic Ca^{2+} responses thus arose through release of Ca^{2+} from intracellular stores. The largest fluorescence ratio signals attained $\Delta\text{F}/\text{F}_0$ values around 10, appreciably below the maximal saturation value of about 19 evoked by ionomycin treatment in cells loaded with Cal520 and imaged by similar protocols to those used here [11]. The experiments in Figs. 1 and 2 were done using different batches of cells. For that reason, and because of differences in the microscope and camera, values of $\Delta\text{F}/\text{F}_0$ and SD signals obtained with the two systems are not directly comparable.

2.5. Image processing and data analysis

Image stacks in nd2 or multi-plane TIF format were imported into FLIKA (<http://flika-org.github.io>), a freely available open-source image processing and analysis software in the Python programming language [24,25]. Internal processing and data output were performed using 64-bit floating-point arithmetic. Processing was performed on image stacks following subtraction of camera black offset level. F/F_0 ratio stacks were then generated by dividing each frame by an average of 100 baseline frames acquired before stimulation and $\Delta\text{F}/\text{F}_0$ image stacks were generated by subtracting 1 from F/F_0 ratio stacks.

To generate image stacks representing the pixel-by-pixel standard deviation (SD) of temporal fluctuations in fluorescence of the Ca^{2+} indicator dye, we used a custom FLIKA script as described previously [10, 11,27]. In brief, following subtraction of camera black offset level, records involving UV flash photolysis were processed using the FLIKA ‘flash remover’ plugin (https://github.com/gddickinson/flika_plugins) to replace the flash artifact with a smooth transition from pre- to post-flash fluorescence levels. The image stack was then spatially filtered by a Gaussian blur function with a standard deviation equivalent to $\sim 1 \mu\text{m}$ at the specimen and was temporally filtered (0.5 to 20 Hz) by a bandpass Butterworth function to attenuate high frequencies of photon shot noise and low frequency shifts in baseline fluorescence. A running variance of this temporally filtered movie was then calculated, pixel by pixel, by subtracting the square of the mean from the mean of the square of a moving 20 frame (160 ms) boxcar window. The running standard deviation was calculated by taking the square root of the variance image stack to create a standard deviation (SD) stack. Finally, to remove the mean predicted photon shot noise (the variance of which increases in linear proportion to the mean fluorescence intensity) the SD stack was corrected, pixel-by-pixel, by subtracting the square root of a running mean of the spatially filtered fluorescence image stack multiplied by a scalar constant. Traces showing changes in SD signal throughout Ca^{2+} responses were measured from a region of interest (ROI) encompassing the entire cell, and from small (4×4 pixel; $1.28 \times 1.28 \mu\text{m}$) ROIs. Amplitudes of SD signals are reported in arbitrary units (AU), that are consistent within experiments using the Evolve camera (Fig. 1) or the iXion camera (Fig. 2). The locations of active puff sites were visualized by forming maximum intensity SD projection images where the intensity of each pixel is the maximum at that pixel across a range of frames acquired during the rising phase of Ca^{2+} responses. The locations of these

ROIs were then transposed onto $\Delta\text{F}/\text{F}_0$ images for quantification of puff amplitudes. Measurements are stated as mean ± 1 SEM.

Data plotting and statistical analysis were done using Microcal Origin (Northampton, Mass.) Mean values are expressed throughout as standardized mean ± 1 s.e.m. Comparison of mean values between groups was assessed by Student’s T-test. Chi squared values evaluating the correspondence between observed and predicted distributions of numbers of channels per site in Fig. 6 were calculated excluding sites with $N \geq 3$ channels where few data were available.

3. Results

3.1. KRAP-knockdown impairs both punctate and diffuse Ca^{2+} liberation

We recently described that global IP_3 -mediated Ca^{2+} signals arise through a combination of two different modes of Ca^{2+} liberation; ‘punctate’ release as transient, localized puffs, together with a spatially and temporally ‘diffuse’ release [10,11]. In light of findings that KRAP selectively localizes and licenses the clustered IP_3Rs that underlie puffs [17] we investigated whether knockdown of KRAP may differentially affect the punctate vs. diffuse modes of Ca^{2+} release. As a convenient measure of punctate release we analyzed temporal fluctuations in Ca^{2+} fluorescence signal, utilizing an algorithm to generate a standard deviation (SD) signal that reflects the mean puff activity throughout the TIRF footprint of a cell [11,24]. Because puff activity contributes $< 30\%$ of the total Ca^{2+} liberation during a global Ca^{2+} response [10,11] measurement of the peak amplitude of the global response then provides an indication of the relative magnitude of diffuse mode Ca^{2+} release. We evaluated the effect of KRAP knockdown on the respective magnitudes of puff activity and peak global signal under two conditions; (i) by examining cell-to-cell variability in responses evoked by a fixed, maximal stimulus, and (ii) by applying photolysis flashes to photo-release varying amounts of i-IP_3 .

In our first approach we stimulated cells by local application of a maximal concentration (100 μM) of histamine. Supplemental Fig. S1A shows superimposed traces of global Ca^{2+} fluorescence signals ($\Delta\text{F}/\text{F}_0$) evoked in control cells and in cells treated with siRNA to knock down KRAP expression. The mean size of the peak global Ca^{2+} signals reduced from $7.12 \pm 0.36 \Delta\text{F}/\text{F}_0$ in 19 control cells to 4.27 ± 0.57 in 21 KRAP knockdown cells (Fig. S1B), and their latencies (time to peak) lengthened from 21.1 ± 2.5 s to 34.2 ± 4.75 s. This relatively modest reduction in mean response amplitudes was appropriate for our purpose to examine whether the level of KRAP equivalently affected different aspects of Ca^{2+} signaling, whereas a strong suppression of signals would yield little information.

Figs. 1A,B compare global Ca^{2+} fluorescence signals ($\Delta\text{F}/\text{F}_0$; red traces) and SD signals (noisy black traces) evoked by local application of a maximal concentration (100 μM) of histamine to individual control and siRNA-treated cells. In parallel with the reduction in mean amplitude of peak global Ca^{2+} signals in the 19 control and 21 KRAP siRNA-treated cells, the mean peak SD signal reduced from 14.25 ± 1.65 to 7.15 ± 1.02 AU. Fig. 1C shows a scatterplot of peak SD signal vs. peak global signal for these control cells (open black symbols) and KRAP knockdown cells (filled red symbols). Both datasets show considerable variability, likely reflecting cell-to-cell variability together with variability in extent of knockdown in the KRAP siRNA-treated cells. Nevertheless, the data points from control and KRAP knockdown cells all lie along the same trend curve, indicating that punctate and diffuse Ca^{2+} release are impaired to a similar extent by diminished KRAP expression.

In our second approach to compare the effects of KRAP knockdown on punctate and global Ca^{2+} release we evoked responses by photo-release of i-IP_3 with UV flashes of varying durations. Figs. 2A,B respectively illustrate records of global Ca^{2+} fluorescence signals ($\Delta\text{F}/\text{F}_0$; red traces) and SD signals (black) evoked by photorelease of i-IP_3 by UV flashes of increasing durations in control cells (Fig. 2A) and KRAP

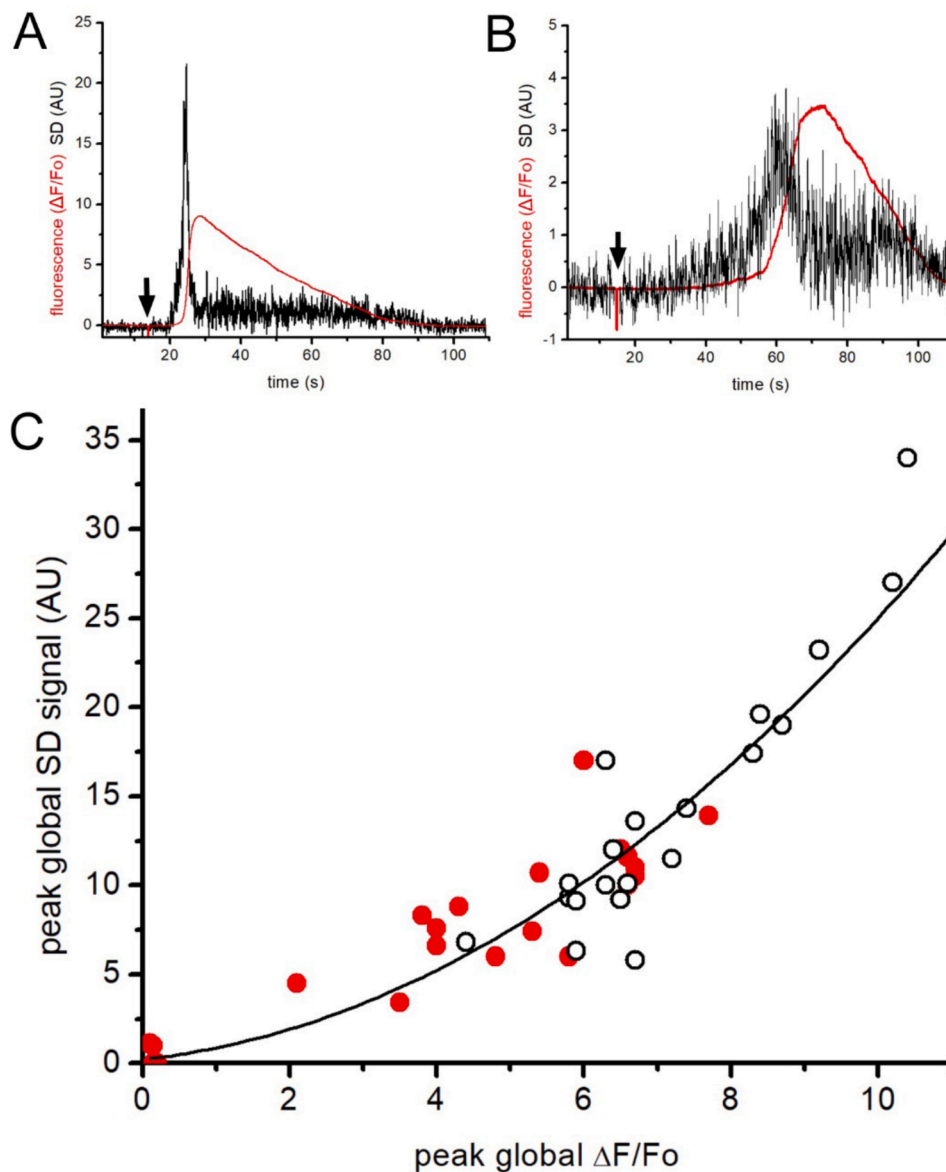


Fig. 1. KRAP knockdown depresses both, punctate and diffuse modes of Ca^{2+} liberation. (A) Global fluorescence ratio Ca^{2+} signal ($\Delta F/F_0$; red trace) and SD signal (noisy black trace) from a representative control HeLa cell stimulated by local application of $100 \mu\text{M}$ histamine when marked by the arrow. (B) Corresponding records from a cell treated with siRNA to reduce expression of KRAP. (C) Scatter plot of peak global SD signal vs. peak global Ca^{2+} signal ($\Delta F/F_0$) for 19 control cells (open black symbols) and 17 KRAP knockdown cells (filled red symbols). The SD signal is expressed in arbitrary camera units, consistent for all data. The curve is a second-power relationship empirically fitted to the composite data.

knockdown cells (Fig. 2B). In both control and KRAP knockdown cells the peak amplitudes of global Ca^{2+} responses and SD signals increased with increasing flash duration, but both signals were smaller in the KRAP knockdown cells for equivalent flash durations. The mean values of peak global $\Delta F/F_0$ response pooled from 100 ms and 200 ms UV flash stimulation were significantly different between control and KRAP siRNA-treated cells ($p = 0.046$; control cell mean = 1.25 ± 1.44 , $n = 17$; KRAP knockdown cell mean = 0.19 ± 0.15 , $n = 6$). Similarly, the mean values of peak global SD responses pooled from 100 ms and 200 ms UV flash stimulation were significantly different between control and KRAP siRNA treated cells ($p = 0.045$; control cell mean = 7.05 ± 46.6 , $n = 17$; KRAP knockdown cell mean = 0.995 ± 0.39 , $n = 6$). The dose/response relationships for global Ca^{2+} signals (Fig. 2C) and SD signals (Fig. 2D) evoked by different flash durations were both depressed and shifted rightward in KRAP knockdown cells, such that a roughly 3–4-fold longer flash duration was required to evoke responses comparable to that in control cells. For example, the mean peak global SD signal evoked by 100 ms flashes in control cells (4.65 ± 7.6 AU, $n = 12$) was not significantly different ($p = 0.21$) from that evoked by 400 s flashes in KRAP knockdown cells (1.42 ± 2.17 AU, $n = 10$). A scatter plot of peak SD signal vs. peak global $\Delta F/F_0$ response (Fig. 2D) revealed a close overlap

between data from control cells (open black symbols) and KRAP knockdown cells (filled red symbols); further indicating that the relative proportions of Ca^{2+} liberation attributable to punctate and diffuse modes was little changed by reduction of KRAP expression.

3.3. Punctate and diffuse Ca^{2+} release in cells expressing single IP_3R isoforms

HeLa cells predominantly express IP_3R types 1 and 3 [13,26]. To examine whether the Ca^{2+} signals remaining in the HeLa KRAP knockdown cells might arise from an IP_3R isoform whose activity is not regulated by KRAP we utilized HEK293 cell lines that were genetically engineered to express exclusively type 1 or type 3 IP_3Rs [27]. Knockdown of KRAP reduced the peak amplitude of global Ca^{2+} signals evoked by local application of $100 \mu\text{M}$ carbachol by 30% in HEK293 cells expressing $\text{IP}_3\text{R}1$ ($\Delta F/F_0$ 3.68 ± 0.31 in control vs. 2.55 ± 0.4 in KRAP knockdown; $n = 8$ –10 cells per condition, $p = 0.048$) and by 43% in $\text{IP}_3\text{R}3$ -expressing cells ($\Delta F/F_0$ 7.56 ± 0.61 in control vs. 4.28 ± 0.55 in KRAP knockdown; $n = 8$ –9 cells per condition, $p = 0.001$). These results demonstrate that KRAP knockdown functionally depresses Ca^{2+} release mediated by both $\text{IP}_3\text{R}1$ and $\text{IP}_3\text{R}3$, findings consistent with prior studies

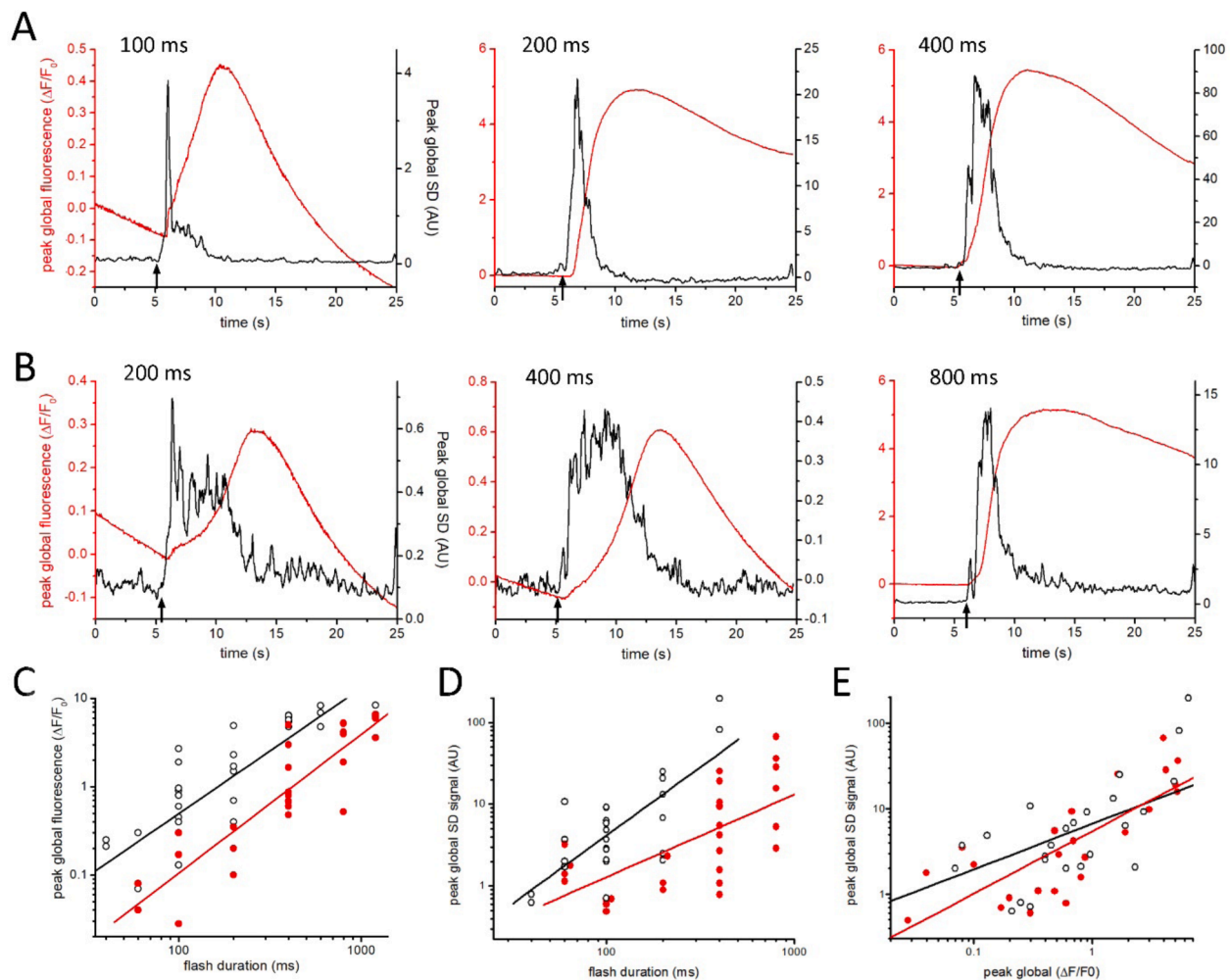


Fig. 2. IP₃-sensitivity of punctate and global Ca²⁺ release is equivalently reduced by KRAP knockdown. (A, B) Examples of global $\Delta F/F_0$ and SD signals evoked by photorelease of ci-IP₃ with varying flash durations as indicated. Each panel is from a different HeLa cell treated with control siRNA (A) or with siRNA to knock down KRAP expression (B). In each panel the $\Delta F/F_0$ trace (red) and SD trace (black) are plotted on different y-axes, individually scaled for presentation so that the peak amplitudes of the traces are roughly similar. (C) Peak global $\Delta F/F_0$ signals evoked in control (black open circles; 36 cells) and KRAP knockdown cells (filled red circles; 29 cells) by photorelease of i-IP₃ by UV flashes of varying durations. (D) Peak global SD signals evoked in control (black open circles) and KRAP knockdown cells (filled red circles) by photorelease of i-IP₃ by UV flashes of varying durations. Control data with flashes >400 ms could not be obtained as the SD signal was obscured by the flash artifact. (E) Scatter plot of peak amplitude of SD signal (punctate activity) vs. peak amplitude of the global Ca²⁺ signal ($\Delta F/F_0$) in that cell. Data are from 26 control cells (black open circles) and 26 KRAP knockdown cells (filled red circles). Data in C-E are plotted on double logarithmic coordinates to better encompass the wide range of stimulus and response amplitudes. Lines are linear regressions fit to the data on double logarithmic axes.

reporting that KRAP co-immunoprecipitates with both types 1 and 3 IP₃Rs [15], and that KRAP silencing disrupts the cellular distributions of IP₃R1 and IP₃R3 [16].

3.4. Imaging the action of KRAP on Ca²⁺ signals from single IP₃R channels

The observations of Thillaiappan et al. [17] suggested that KRAP licenses a cluster of IP₃Rs to respond to IP₃ as a single functional entity to generate puffs, rather than licensing individual IP₃Rs within a cluster. Specifically, they reported that the number of sites evoking puffs within a cell increased with increasing levels of KRAP over-expression, whereas the mean amplitude of puffs at these sites - a measure of the number of IP₃R channels opening within a cluster - appeared independent of the level of KRAP. Further, they described that knockdown of KRAP resulted in almost complete abolition of local Ca²⁺ signals. However, we suspected that small fluorescence signals (blips) [18,28] generated by openings of individual IP₃R channels remaining after KRAP knockdown might have escaped detection. The automated algorithm (FLIKA) used

by Thillaiappan et al. to identify puffs was developed in our lab [24,25] and we are aware of its limitations in detecting signals close to the baseline noise level, even with adjustments of threshold level as performed by Thillaiappan et al. [17]. To enhance the detection sensitivity, we therefore recorded from cells that were loaded with cytosolic EGTA to sharpen local Ca²⁺ signals and suppress global rises in baseline Ca²⁺ [7,29], and employed fluctuation analysis to identify local Ca²⁺ transients with a signal-to-noise ratio better than that of the 'raw' fluorescence signal [10,30].

The panels in Fig. 3A,B and supplemental Fig. S3 show representative SD images that depict, for each pixel, the standard deviation of Ca²⁺-dependent temporal fluctuations in fluorescence. Each panel is a maximum-intensity projection across 1000 frames (8 s) acquired after photorelease of i-IP₃. Bright regions highlight sites of transient, local Ca²⁺ events occurring during this time. SD images from control cells exhibited several bright hot-spots evoked following photorelease of i-IP₃, corresponding to sites generating large puffs, together with numerous other sites showing weaker SD signals. In KRAP knockdown cells the evoked local Ca²⁺ activity was greatly diminished, but several

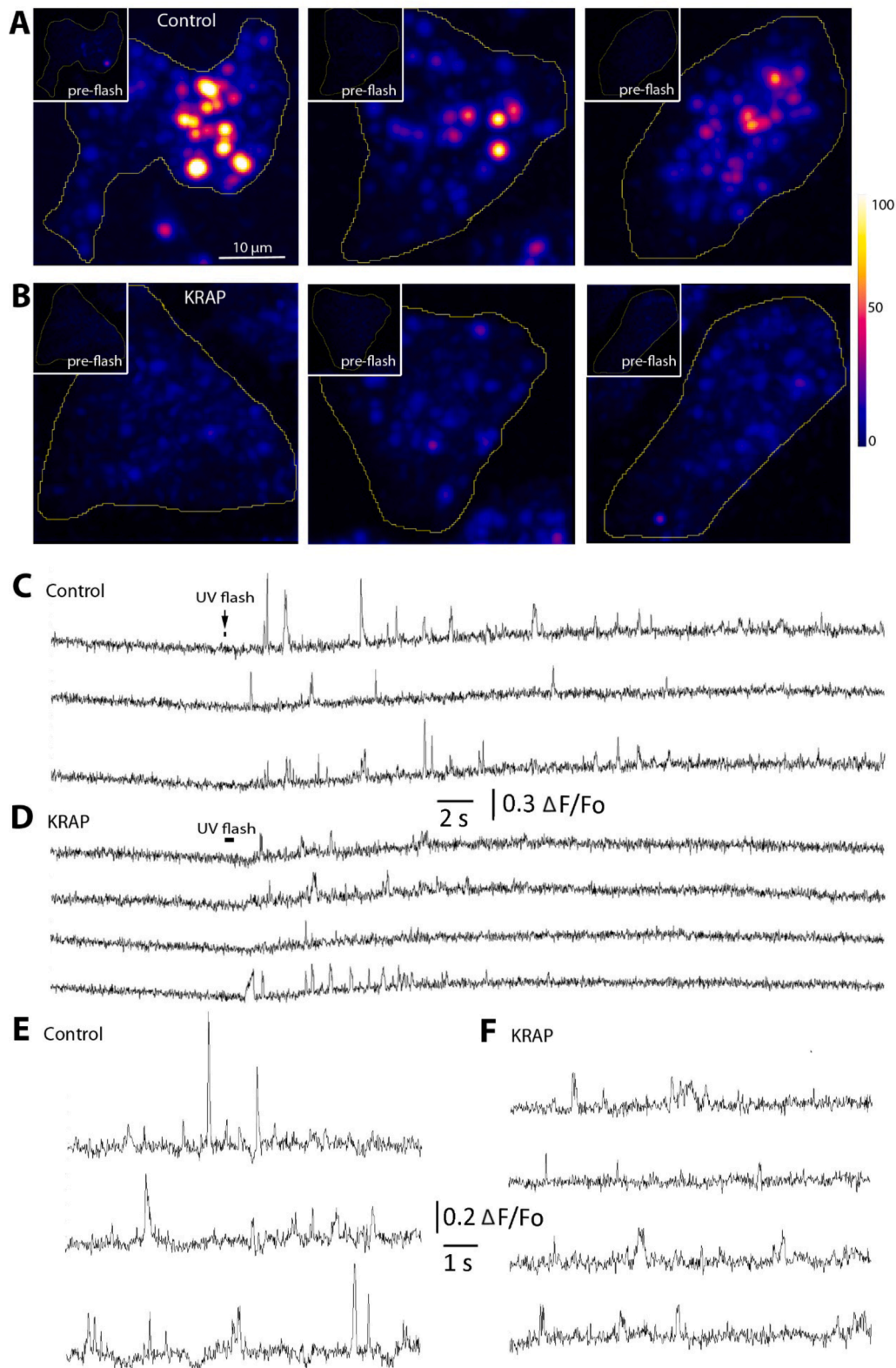


Fig. 3. KRAP knockdown cells predominantly show single channel Ca^{2+} signals (blips). (A) Three examples of maximum projection SD images of 1000 frames (8 s) acquired following photorelease of $i\text{-IP}_3$ by a 25 ms flash duration in 3 control siRNA treated cells. Insets show baseline maximum intensity SD projections before stimulation. (B) Corresponding images from 3 KRAP siRNA-treated cells, following photorelease of $i\text{-IP}_3$ with 200 ms (left two cells) and 400 ms (right cell) flash durations. The inset pre-flash images are reproduced at full size in supplemental Fig. S3. (C,D) Representative traces of fluorescence signals ($\Delta F/F_0$) recorded, respectively, in control and KRAP knockdown cells from small ROIs (4×4 pixel) placed on active hotspots identified from images like those in A,B. (E,F) Traces shown on an expanded timescale to better illustrate the kinetics of Ca^{2+} signals in control (E) and KRAP knockdown cells (F).

sites showing weak, localized SD signals remained evident in each cell.

3.5. KRAP knockdown reduces the numbers of responding IP₃R channels but not the single-channel Ca²⁺ flux

To measure local Ca²⁺ fluorescence events we used SD image stacks and maximum intensity SD projections to identify hot-spots as a guide to position small regions of interest (ROIs) on image stacks of fluorescence ratio signal ($\Delta F/F_0$). Supplemental Video 1 shows representative image stacks of fluorescence (upper panels) and SD signal (lower panels) from a control cell (left) and a KRAP knockdown cell (right). Control cells generated local puffs (Fig. 3C,E) with varying amplitudes ranging as high as 2.3 $\Delta F/F_0$, together with smaller events ($\Delta F/F_0 < 0.2$) compatible with blips arising from openings of single IP₃R channels [31–33]. In contrast KRAP-knockdown cells showed predominantly small ($\Delta F/F_0 < 0.2$), blip-like signals (Figs. 3D,F), and no events were observed with amplitudes $> 0.4 \Delta F/F_0$. The mean amplitude of events in control cells was $\Delta F/F_0 0.263 \pm 0.009$ (6 cells, 1228 events) versus 0.152 ± 0.003 (10 cells, 1130 events) in KRAP knockdown cells. The observed mean numbers of events per site during the recording period were similar in control (4.22) and in KRAP knockdown cells (3.88).

Figs. 4A, B respectively plot the amplitude distributions of all events observed in control and KRAP-knockdown cells. The data from control cells (Fig. 4A) displayed a multi-modal distribution, resembling that described previously for local IP₃-evoked Ca²⁺ signals in several cell types [31–33]. The peak amplitudes of Gaussian components fitted to the data recurred at roughly integer multiples, reflecting the coordinated openings of 1,2,3,4 etc. IP₃R channels within a cluster [33]. The number of events under the first Gaussian component was 51% of the total (627/1228), indicating that about one half of all events in control cells likely involved openings of single channels, with multi-channel puffs comprising the remainder. Different from this, the amplitudes of events in KRAP knockdown cells were largely distributed as a single Gaussian function (Fig. 4B), with single-channel blips representing 91% (1113/1026) of all events.

The mean of a Gaussian function fitted to the first peak of the KRAP knockdown data (mean $\Delta F/F_0$ of 0.129) was similar to that of the first peak of the control data (mean $\Delta F/F_0$ of 0.144); with both values consistent with earlier measurements of fluorescence signals generated by openings of single IP₃R channels [31–33]. In EGTA-loaded cells imaged by TIRF microscopy the fluorescence ratio ($\Delta F/F_0$) of local Ca²⁺

signals provides a relative measure of the Ca²⁺ flux (current) through the channel. We thus interpret these results as indicating that the Ca²⁺ flux through individual open IP₃R channels was little affected by knockdown of KRAP. On the other hand, the proportion of events involving the concerted opening of multiple channels was substantially lower in KRAP knockdown cells (9% vs 49% in controls).

3.6. Estimating the number of functional channels at a site

The reduced proportion of multi-channel events in KRAP knockdown cells may reflect both changes in the mean numbers of functional channels present per site, and in the frequency at which events of differing magnitudes arise. To estimate the minimum number of functional channels present at any given site we measured the amplitude of the largest event observed at that site [10]. In control cells ($n = 6$) the distribution of sites generating events of a given maximal amplitude could again be fitted by a multimodal distribution, with Gaussian peaks distributed at roughly integer steps corresponding to sites where maximal events involved the concerted opening of 1,2,3 etc. channels (Fig. 5A). The corresponding data in KRAP knockdown cells ($n = 10$) predominantly followed a single Gaussian distribution, corresponding to single-channel events, with a smaller Gaussian component at an amplitude ($\Delta F/F_0 0.26$) corresponding to two-channel events (Fig. 5B). The mean maximum event size in control cells was $\Delta F/F_0 0.425$ as compared to 0.180 in KRAP knockdown cells, a reduction to 42%.

By taking the areas under the Gaussian components in Figs. 5A,B, we then derived the mean numbers of sites that contained N (1, 2, 3 etc.) functional channels within the TIRF footprint of control (Fig. 5C) and KRAP knockdown cells (Fig. 5D). In control cells we observed a mean of 51.0 functional sites per cell and estimated a mean of 123 functional channels per cell, giving an average number of channels per site of 2.41. In KRAP knockdown cells we observed a mean of 31.8 functional sites per cell, indicating that an average of about 19 sites (51 minus 32) per cell had become ‘silenced’ by the reduced expression of KRAP. The mean number of functional channels per cell was 41, giving an average number of functional channels per site (including silenced sites) of 0.8; a reduction by 66% as compared to control cells

3.7. KRAP licenses individual IP₃R channels not individual clusters

We considered three models by which lack of KRAP might result in

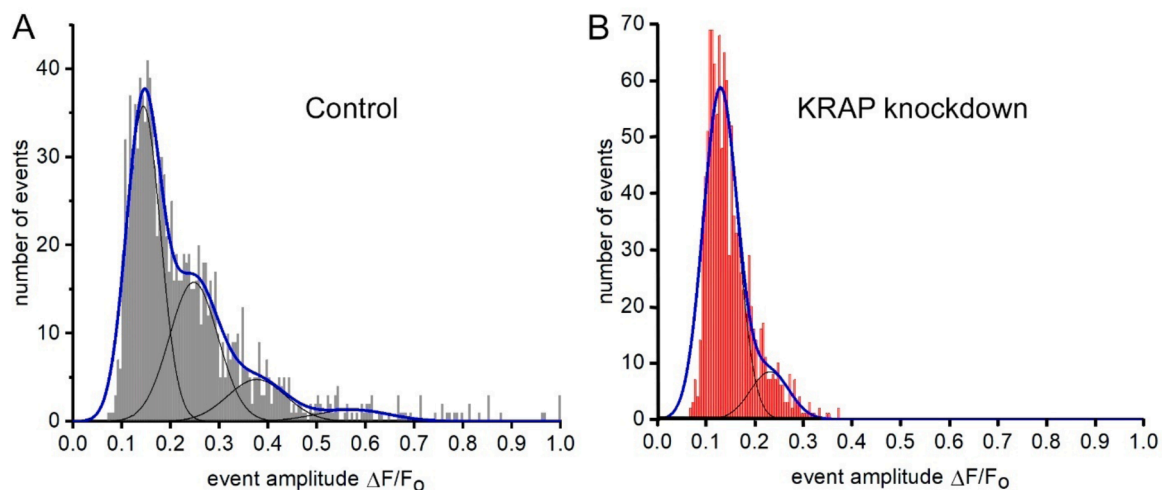


Fig. 4. Amplitude distributions of local Ca²⁺ events in control and KRAP knockdown cells. (A) Distribution of peak amplitudes of all local Ca²⁺ events ($n = 1226$) in 6 cells treated with control siRNA. The x-axis is truncated at 1.0 $\Delta F/F_0$ and omits 16 events with amplitudes between 1.03 and 2.3 $\Delta F/F_0$. The blue curve is a four-component Gaussian fit to the data, with respective means of individual Gaussian distributions (black curves) of $\Delta F/F_0 0.144, 0.248, 0.377$ and 0.573 and areas of 627, 396, 143 and 50 events. (B) Distribution of event amplitudes in KRAP siRNA-treated cells. Data are from 1130 events in 10 cells. Curves show a two-component Gaussian fit to the data, with means of $\Delta F/F_0 0.129$ and 0.231 .

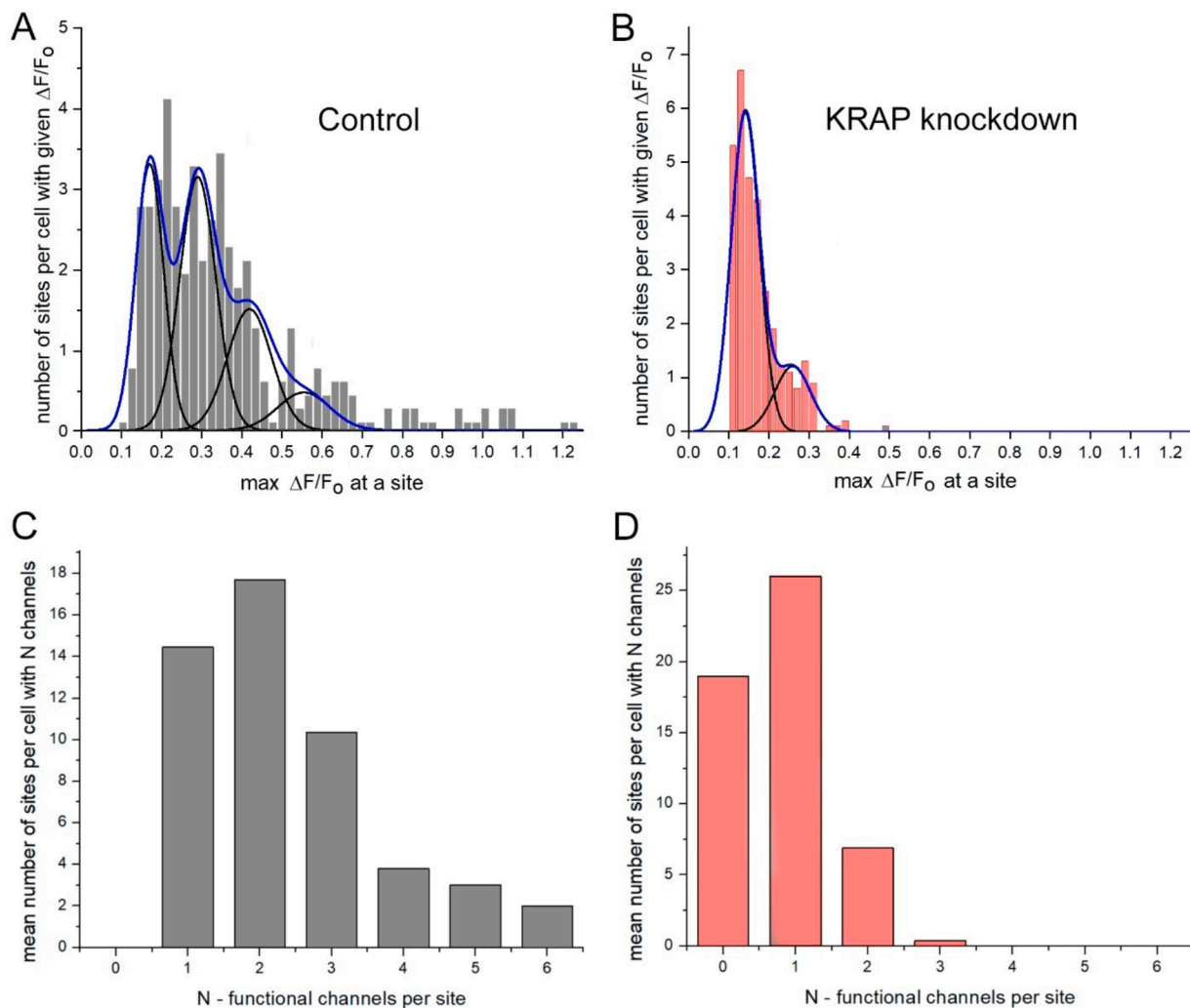


Fig. 5. Distributions of sites containing differing numbers of IP₃R channels in control and KRAP knockdown cells. (A) Distributions of largest event amplitudes among 6 control cells. The y-axis is scaled as the mean number of sites per cell showing events of a given amplitude. The blue curve shows the sum of 4 Gaussian functions fitted to the data (black curves) with means of $\Delta F/F_0$ 0.170, 0.290, 0.419 and 0.554. The mean number of sites per cell was 51. (B) Corresponding distribution of largest event sizes among 10 cells treated with KRAP siRNA. The means of the Gaussian distributions are $\Delta F/F_0$ 0.141 and 0.259, and the mean number of observed sites per cell was 32. (C, D) Bar graphs show, respectively, for control and KRAP knockdown cells, the estimated mean numbers of sites per cell containing N channels. Values were derived from the areas under the Gaussian curves in A, B, and by manually counting the numbers of sites estimated to contain ≥ 5 channels in control cells. The mean number of sites (19) with zero functional channels in KRAP knockdown cells was derived from the difference in mean numbers of functional sites in control (51) and KRAP knockdown cells (32). The estimated mean total number of functional channels per control cell was 123, and in KRAP knockdown cells 41; a reduction by 66%.

the marked reduction in numbers of functional channels and the associated change in distributions of sites containing differing numbers of channels (Figs. 5C,D). (i) KRAP knockdown randomly silenced individual sites, with uniform probability regardless of how many channels they contained. (ii) KRAP knockdown randomly silenced multi-channel sites, while sparing a discrete population of lone channel sites that did not require KRAP to function. (iii) KRAP knockdown randomly silenced individual IP₃R channels with equal probability across all sites. To discriminate between these scenarios, we predicted the mean numbers of sites per cell containing N channels that would remain if the observed functional sites or channels in control cells (Fig. 5A) were silenced according to each model, and compared these with the observed distribution in KRAP knockdown cells. The cyan bars in Figs 6A,B,C show the respective predictions. Red bars show, for comparison, the observed data replotted from Fig. 5D. In all three models the parameter value for the probability of silencing a site or channel was adjusted so that the predicted mean number of functional channels per cell matched the observed number (41). The predicted number of completely silenced

sites ($N = 0$) was taken as the difference between the mean number of observed sites per control cell minus that in KRAP knockdown cells.

Model (i) - random silencing of 66% of sites (Fig. 6A) - yielded a poor fit to the observations (Chi-squared value = 128). Notably, that model predicted nearly twice as many completely silenced sites ($N = 0$) as observed, but only about one fifth as many single channel sites ($N = 1$). Model (ii) - random silencing of 75% of multi-channel sites (Fig. 6B) - gave only a moderately improved fit (Chi-squared value = 16), again predicting a considerable excess of silenced sites, and a lower number of single channel sites. On the other hand, model (iii) - stochastic silencing of 66% of individual channels (Fig. 6C) - provided a substantially better fit to the data (Chi-squared value = 1.4).

3.8. Availability of KRAP stochastically determines the number of functional IP₃Rs in a cluster

The improved fit provided by model (iii) suggested that KRAP may stochastically and independently license individual IP₃R channels

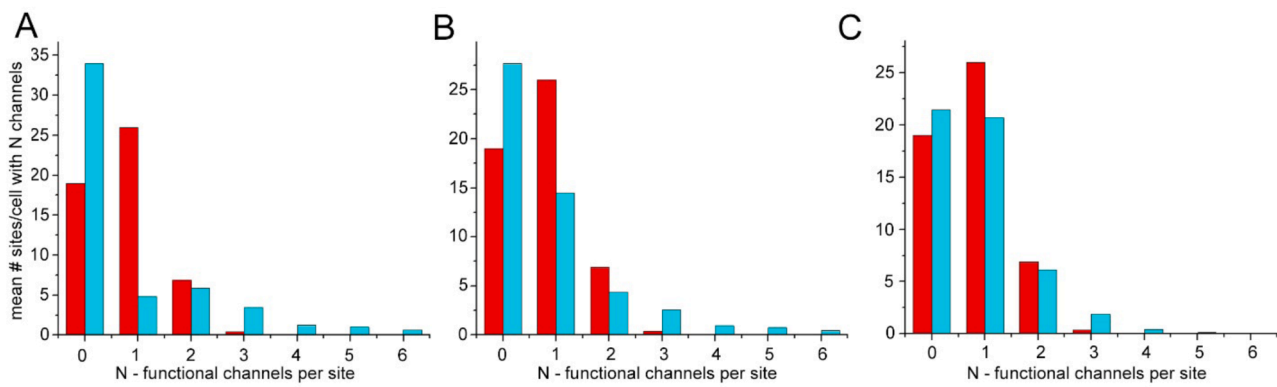


Fig. 6. Modeling the predicted distributions of sites containing differing numbers of IP₃R channels in KRAP knockdown cells. In all panels, the red bars show the mean number of sites per KRAP knockdown cell estimated to contain $N = 0, 1, 2, 3, 4, 5, 6$ channels, reproduced from Fig. 5D. Cyan bars show the mean numbers of sites per cell predicted by different models for the action of KRAP on puff sites or individual IP₃R channels. (A) Distribution predicted by a model in which lack of KRAP results in silencing of 66% of the functional sites present in control cells. (B) Distribution predicted by a model in which lack of KRAP results in silencing of 75% of the multi-channel sites present in control cells but leaves unaffected those sites containing a single channel. (C) Distribution predicted by a model in which lack of KRAP results in the random silencing of 75% of individual IP₃R channels.

within clusters, so that the mean number of functional channels per cluster, m , is determined by the level of KRAP expression. To evaluate this possibility, we examined whether the numbers of functional channels per site in both control and KRAP knockdown cells were distributed following Poisson statistics, as expected for a stochastic distribution. The probability distribution of the Poisson function requires only a single parameter, m . In the case of the control cells we could not calculate m directly from the mean of the observed data in Fig. 5A, because this may have been biased by omission of undetected, silent sites. Instead, we adjusted parameter values for m and the number of silent sites, obtaining an optimal fit to the data for observed sites ($N \geq 1$) with $m = 2.236$ and a predicted mean of 6 silent sites per cell (Fig. 7A). In the case of the KRAP knockdown cells the data were fit (Fig. 7B) by a Poisson relationship with $m = 0.745$, determined from a total mean number of sites per cell = 56 (33 functional sites + 23 silent sites).

4. Discussion

Numerous proteins have been identified to associate with IP₃Rs and potentially modulate their localization and/or their function to release

Ca²⁺ in response to IP₃ [34]. Here, we focused on KRAP, a cytoplasmic protein associated with filamentous-actin [14]. KRAP was initially shown to be relevant to the localization of IP₃Rs [16], and to be crucial for their functioning because knockdown of KRAP in HEK293 cells diminished IP₃-mediated Ca²⁺ release without affecting the content of intracellular Ca²⁺ stores or the binding of IP₃ to its receptor [15]. A more recent study by Thillaiappan et al. [17] reinforced the functional importance of KRAP, reporting that essentially all IP₃-evoked responses in HeLa cells could be eliminated by knockdown of KRAP without changing the expression level of IP₃Rs, and concluded that endogenous KRAP limits the number of IP₃Rs licensed to respond to IP₃ and thereby the ability of a cell to evoke cytosolic Ca²⁺ signals. Moreover, Thillaiappan et al. [17] derived additional mechanistic insights, showing that KRAP tethered loose confederations of IP₃Rs to actin filaments immediately beneath the plasma membrane to establish the stationary clusters of IP₃Rs that generate local Ca²⁺ puffs. Here, we investigated whether KRAP regulates the ability of clustered IP₃Rs to generate puffs by licensing individual receptor/channels or the cluster as a unitary entity; and whether KRAP is equivalently required for diffuse, cell-wide Ca²⁺ release by IP₃.

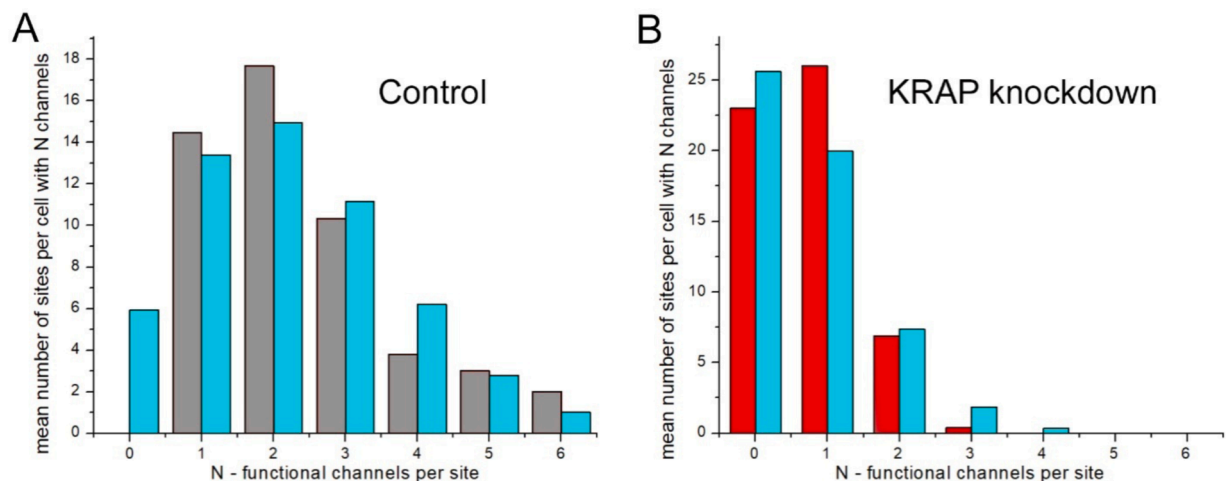


Fig. 7. The distributions of sites containing differing numbers of functional channels in control and KRAP knockdown cells accord with Poisson relationships. Cyan bars show Poisson distributions fitted to the observed distributions of numbers of sites containing N functional channels in control (A) and KRAP knockdown cells (B). gray and red bars respectively reproduce the observed data from Figs. 5C, D. The control distribution was calculated with the mean number of channels per site = 2.236, and with the predicted number of undetected, silent sites = 6. The KRAP knockdown distribution was calculated with the mean number of channels per site = 0.745, and with the predicted number of undetected, silent sites = 26.

4.1. Licensing of IP₃Rs at puff sites by KRAP

The IP₃Rs at puff sites represent only a small fraction of all those present in the cell, leading to proposals that some unidentified factor enables these clustered receptors to preferentially respond to low levels of IP₃ [5,6]. Our findings here confirm and extend the results of Thillaiappan et al. [17] in showing that KRAP is required for the gating of IP₃Rs within clusters. We found that mean size of local Ca²⁺ puffs was strongly reduced by KRAP knockdown, whereas the amplitude of Ca²⁺ signals attributable to openings of single IP₃R channels was little affected. Thus, KRAP appeared to control the number of licensed IP₃R channels at a puff site, but not the Ca²⁺ flux through those channels that do open. To quantify this effect, we estimated the numbers of functional IP₃Rs present at a puff site by scaling the amplitude of the largest Ca²⁺ event at that site as an integer multiple of the signal generated by the opening of a single IP₃R channel. In control cells expressing physiological levels of KRAP, and in cells where expression of KRAP had been reduced by siRNA treatment, the estimated numbers of functional channels per site (1, 2, 3 etc.) followed a distribution in good accord with Poisson statistics, indicating a stochastic variation in the small numbers of channels active within different sites across the cell. Notably, however, the mean number of functional channels per site was reduced to about one third in the KRAP knockdown cells. Thus, we conclude that the level KRAP plays a key role in stochastically titrating how many licensed channels are present at a site.

Our observation of small Ca²⁺ events in KRAP knockdown cells, predominantly attributable to openings of single IP₃R channels, differs from the report by Thillaiappan et al. [17] that local Ca²⁺ signals were completely abolished by KRAP knockdown. These conflicting results may have resulted in part from differing levels of KRAP knockdown, as we imaged 48 hrs after transfection of siRNA, whereas Thillaiappan et al. imaged after 72 hrs. In addition, the failure of Thillaiappan et al. to detect residual activity may be ascribed to the slower imaging rate they used (20 frames s⁻¹ versus 125 frames s⁻¹ in our studies), together with the lower sensitivity of the algorithm they used to threshold events as compared to our method of fluctuation analysis. Indeed, careful inspection of the published video record of Thillaiappan et al. (supplemental video 8) [17] does appear to reveal local Ca²⁺ events in the KRAP knockdown cell. We propose that residual events in our studies, and likely in those of Thillaiappan et al., persisted because KRAP levels were not completely knocked down and reject an alternative hypothesis that the cells may have expressed a distinct population of 'lone' IP₃R channels that do not require KRAP to function. Specifically, the numbers and amplitude distribution of residual events we observed accorded well with that predicted if lack of KRAP were to stochastically silence individual IP₃R channels within a cluster, one-by-one; but not with that expected if reduced levels of KRAP were to selectively silence individual multi-channel sites.

In contrast to our conclusion that KRAP determines the number of functional channels within a puff site at physiological and sub-physiological levels, Thillaiappan et al. [17] described that overexpression of KRAP increased the numbers of puff sites per cell without affecting the mean amplitude of puffs; suggesting that the availability of KRAP determines, in an all-or-none manner, the responsiveness of IP₃R clusters as unitary entities without affecting the average numbers of functional channels within a cluster. We suspect that these differences in findings and interpretations may have a straightforward methodological explanation. A lower detection sensitivity in the experiments of Thillaiappan et al. would lead to an undercount of the number of active puff sites in control cells and bias the estimated mean puff amplitude higher than the true value. Licensing of an increased number of individual IP₃Rs by overexpression of KRAP would then result in detection of previously undetected sites that now contained sufficient functional channels to produce supra-threshold responses. Further, it is likely that a factor (such as the availability of IP₃R anchoring sites in a scaffolding structure) [35] sets an upper bound to the number of IP₃Rs that can be

physically present in a cluster. Thus, the amplitudes of detected events would be constrained between the detection threshold and that set by the maximal number of IP₃Rs; a limited range that might obscure an increase in puff amplitudes resulting from overexpression of KRAP.

In addition to examining the requirement of KRAP for IP₃R function, Thillaiappan et al. further utilized expression of EGFP-tagged IP₃R show that knockdown of KRAP reduced the number of immotile IP₃R puncta adjacent to the plasma membrane [17]. They ascribed this to a loss of bright puncta rather than disaggregation of individual IP₃R puncta; supporting a notion that KRAP both licenses IP₃Rs within a cluster and anchors the cluster to actin as a unit. Their observation may be reconciled with our finding that KRAP licenses individual IP₃Rs by a model where a scaffolding structure determines the number of IP₃Rs physically present within a punctum (cluster) [17, 35]. The availability of KRAP then determines how many of these receptors are licensed by binding KRAP, and we suggest that the presence of even a single KRAP-associated IP₃R is sufficient to anchor a cluster. Reductions of KRAP level would then progressively reduce the number of licensed IP₃Rs in a cluster without changing the number physically present (the brightness of a punctum), up until the point where no IP₃R bound KRAP and the cluster became unmoored.

4.2. Dependence of diffuse IP₃-evoked Ca²⁺ release on KRAP

We recently proposed that global, cell wide Ca²⁺ signals mediated by IP₃ are composed from two different modes of Ca²⁺ liberation from the ER. Local puff activity ('punctate' Ca²⁺ liberation) largely terminates about mid-way during the rise of global Ca²⁺ spikes, whereas a greater fraction of the total Ca²⁺ release originates through a distinct, 'diffuse' mode of Ca²⁺ release [10,11]. In agreement with previous reports [15, 17] we found that KRAP knockdown strongly attenuated global Ca²⁺ responses. The extent of attenuation roughly paralleled the attenuation of puff activity, indicating that KRAP is equivalently required for both punctate and diffuse modes of Ca²⁺ release. Thillaiappan et al. [17] proposed that the suppression of global Ca²⁺ responses by knockdown of KRAP arises as a consequence of the suppression of puffs, because puffs act as a requisite trigger to evoke diffuse Ca²⁺ release. We argue that this is not the case, because diffuse release can be evoked in conditions such as partial depletion of ER Ca²⁺ content when puff activity is completely suppressed [11]. Instead, we propose that KRAP is required to functionally license the IP₃Rs that underlie both punctate and diffuse Ca²⁺ release.

Together with other findings in immortal cell lines [15–17], our results point to a crucial, indeed likely essential, role for KRAP in enabling Ca²⁺ release through IP₃Rs. However, it is not clear whether this requirement applies universally across all cell and tissue types. Notably, dual knockout of IP₃R isoforms in transgenic mice results in embryonic lethality [36, 37], whereas KRAP knockout mice are viable [38]. Moreover, as previously noted [17], IP₃Rs remain functional in experimental conditions such as patch-clamp recordings and lipid bilayer reconstitution where KRAP would be absent, suggesting that in intact cells KRAP may relieve IP₃Rs from inhibition by some unknown repressor. Variation in expression level of this repressor might thus allow cells to escape from the requirement for KRAP to enable functional IP₃R-mediated Ca²⁺ signaling.

CRediT authorship contribution statement

Irene Vorontsova: Investigation, Visualization, Writing – review & editing, Methodology, Formal analysis. **Jeffrey T. Lock:** Methodology, Writing – review & editing, Formal analysis, Investigation, Visualization. **Ian Parker:** Conceptualization, Methodology, Software, Supervision, Writing – original draft, Writing – review & editing, Formal analysis, Investigation, Visualization, Project administration, Funding acquisition.

Declaration of Competing Interest

None of the authors have any conflict of interest to declare.

Data Availability

Data will be made available on request.

Acknowledgements

We thank Dr. George Dickinson for writing image processing routines and helping with image analysis in FLIKA. This work was supported by the National Institutes of Health grant R37 GM 048071.

Supplementary materials

Supplementary material associated with this article can be found, in the online version, at [doi:10.1016/j.ceca.2022.102638](https://doi.org/10.1016/j.ceca.2022.102638).

References

- M.J. Berridge, Inositol trisphosphate and calcium signalling, *Nature* 361 (1993) 315–325, <https://doi.org/10.1038/361315a0>.
- Ilya Bezprozvanny, J. Watras, B.E. Ehrlich, Bell-shaped calcium-response curves of Ins(1,4,5)P₃- and calcium-gated channels from endoplasmic reticulum of cerebellum, *Nature* 351 (1991) 751–754.
- M. Iino, Biphasic Ca²⁺ dependence of inositol 1,4,5-trisphosphate-induced Ca release in smooth muscle cells of the guinea pig taenia caeci, *J. Gen. Physiol.* 95 (1990) 1103–1122, <https://doi.org/10.1085/jgp.95.6.1103>.
- I. Parker, I. Ivorra, Inhibition by Ca²⁺ of inositol trisphosphate-mediated Ca²⁺ liberation: a possible mechanism for oscillatory release of Ca²⁺, *Proc. Natl. Acad. Sci.* 87 (1990) <https://doi.org/10.1073/pnas.87.1.260>, 260 LP–264.
- I.F. Smith, D. Swaminathan, G.D. Dickinson, I. Parker, Single-molecule tracking of inositol trisphosphate receptors reveals different motilities and distributions, *Biophys. J.* 107 (2014) 834–845, <https://doi.org/10.1016/j.bpj.2014.05.051>.
- N.B. Thillaiappan, A.P. Chavda, S.C. Tovey, D.L. Prole, C.W. Taylor, Ca²⁺ signals initiate at immobile IP₃ receptors adjacent to ER-plasma membrane junctions, *Nat. Commun.* 8 (2017) 1505, <https://doi.org/10.1038/s41467-017-01644-8>.
- I.F. Smith, S.M. Wiltgen, I. Parker, Localization of puff sites adjacent to the plasma membrane: functional and spatial characterization of Ca²⁺ signaling in SH-SY5Y cells utilizing membrane-permeant caged IP₃, *Cell Cal.* 45 (2009) 65–76, <https://doi.org/10.1016/j.ceca.2008.06.001>.
- M.D. Bootman, M.J. Berridge, P. Lipp, Cooking with calcium: the recipes for composing global signals from elementary events, *Cell* 91 (1997) 367–373, [https://doi.org/10.1016/S0092-8674\(00\)80420-1](https://doi.org/10.1016/S0092-8674(00)80420-1).
- N. Callamaras, J.S. Marchant, X.-P. Sun, I. Parker, Activation and co-ordination of InsP₃-mediated elementary Ca²⁺ events during global Ca²⁺ signals in Xenopus oocytes, *J. Physiol.* 509 (1998) 81–91, <https://doi.org/10.1111/j.1469-7793.1998.081bo.x>.
- J.T. Lock, I. Parker, Termination of Ca²⁺ puffs during IP₃-evoked global Ca²⁺ signals, *Cell Cal.* 100 (2021), 102494, <https://doi.org/10.1016/j.ceca.2021.102494>.
- J.T. Lock, I. Parker, IP₃ mediated global Ca²⁺ signals arise through two temporally and spatially distinct modes of Ca²⁺ release, *Elife* 9 (2020) e55008, <https://doi.org/10.7554/eLife.55008>.
- J.S. Marchant, I. Parker, Role of elementary Ca²⁺ puffs in generating repetitive Ca²⁺ oscillations, *EMBO J* 20 (2001) 65–76.
- S.C. Tovey, P. de Smet, P. Lipp, D. Thomas, K.W. Young, L. Missiaen, H. De Smedt, J.B. Parys, M.J. Berridge, J. Thuring, A. Holmes, M.D. Bootman, Calcium puffs are generic InsP₃-activated elementary calcium signals and are downregulated by prolonged hormonal stimulation to inhibit cellular calcium responses, *J. Cell Sci.* 114 (2001) 3979–3989.
- J. Inokuchi, M. Komiya, I. Baba, S. Naito, T. Sasazuki, S. Shirasawa, Deregulated expression of KRAP, a novel gene encoding actin-interacting protein, in human colon cancer cells, *J. Hum. Genet.* 49 (2004) 46–52, <https://doi.org/10.1007/s10038-003-0106-3>.
- T. Fujimoto, T. Machida, T. Tsunoda, K. Doi, T. Ota, M. Kuroki, S. Shirasawa, KRAS-induced actin-interacting protein regulates inositol 1,4,5-trisphosphate-receptor-mediated calcium release, *Biochem. Biophys. Res. Commun.* 408 (2011) 214–217, <https://doi.org/10.1016/j.bbrc.2011.03.112>.
- T. Fujimoto, T. Machida, T. Tsunoda, K. Doi, T. Ota, M. Kuroki, S. Shirasawa, Determination of the critical region of KRAS-induced actin-interacting protein for the interaction with inositol 1,4,5-trisphosphate receptor, *Biochem. Biophys. Res. Commun.* 408 (2011) 282–286, <https://doi.org/10.1016/j.bbrc.2011.04.016>.
- N.B. Thillaiappan, H.A. Smith, P. Atakpa-Adaji, C.W. Taylor, KRAP tethers IP₃ receptors to actin and licenses them to evoke cytosolic Ca²⁺ signals, *Nat. Commun.* 12 (2021) 4514, <https://doi.org/10.1038/s41467-021-24739-9>.
- I. Parker, J. Choi, Y. Yao, Elementary events of InsP₃-induced Ca²⁺ liberation in Xenopus oocytes: hot spots, puffs and blips, *Cell Cal.* 20 (1996) 105–121, [https://doi.org/10.1016/S0143-4160\(96\)90100-1](https://doi.org/10.1016/S0143-4160(96)90100-1).
- M.J. Berridge, Elementary and global aspects of calcium signalling, *J. Physiol.* 499 (1997) 291–306, <https://doi.org/10.1113/jphysiol.1997.sp021927>.
- M.D. Bootman, M.J. Berridge, Subcellular Ca²⁺ signals underlying waves and graded responses in HeLa cells, *Curr. Biol.* 6 (1996) 855–865, [https://doi.org/10.1016/S0960-9822\(02\)00609-7](https://doi.org/10.1016/S0960-9822(02)00609-7).
- M. Bootman, E. Niggli, M. Berridge, P. Lipp, Imaging the hierarchical Ca²⁺ signalling system in HeLa cells, *J. Physiol.* 499 (1997) 307–314, <http://www.ncbi.nlm.nih.gov/pmc/articles/PMC1159306/>.
- S.P. Dawson, J. Keizer, J.E. Pearson, Fire–diffuse–fire model of dynamics of intracellular calcium waves, *Biochemistry* 96 (1999) 6060–6063, <https://doi.org/10.1073/pnas.96.11.6060>.
- J. Marchant, N. Callamaras, I. Parker, Initiation of IP₃-mediated Ca²⁺ waves in Xenopus oocytes, *EMBO J* 18 (1999) 5285–5299, <https://doi.org/10.1093/emboj/18.19.5285>.
- K.L. Ellefsen, J.T. Lock, B. Settle, C.A. Karsten, I. Parker, Applications of FLIKA, a Python-based image processing and analysis platform, for studying local events of cellular calcium signaling, *Biochim. Biophys. Acta - Mol. Cell Res.* 1866 (2019) 1171–1179, <https://doi.org/10.1016/j.bbamcr.2018.11.012>.
- K.L. Ellefsen, B. Settle, I. Parker, I.F. Smith, An algorithm for automated detection, localization and measurement of local calcium signals from camera-based imaging, *Cell Cal.* 56 (2014) 147–156, <https://doi.org/10.1016/j.ceca.2014.06.003>.
- M. Hattori, A.Z. Suzuki, T. Higo, H. Miyauchi, T. Michikawa, T. Nakamura, T. Inoue, K. Mikoshiba, Distinct roles of inositol 1,4,5-trisphosphate receptor types 1 and 3 in Ca²⁺ signaling, *J. Biol. Chem.* 279 (2004) 11967–11975, <https://doi.org/10.1074/jbc.M311456200>.
- K.J. Alzayady, L. Wang, R. Chandrasekhar, L.E.W. Ii, F. Van Petegem, D.I. Yule, Defining the stoichiometry of inositol 1,4,5-trisphosphate binding required to initiate Ca²⁺ release, *Sci. Signal.* 9 (2016) 1–12, <http://stke.sciencemag.org/content/9/422/ra35.abstract>.
- G.D. Dickinson, I. Parker, Factors determining the recruitment of inositol trisphosphate receptor channels during calcium puffs, *Biophys. J.* 105 (2013) 2474–2484, <https://doi.org/10.1016/j.bpj.2013.10.028>.
- S.L. Dargan, I. Parker, Buffer kinetics shape the spatiotemporal patterns of IP₃-evoked Ca²⁺ signals, *J. Physiol.* 553 (2003) 775–788, <https://doi.org/10.1113/jphysiol.2003.054247>.
- D. Swaminathan, G.D. Dickinson, A. Demuro, I. Parker, Noise analysis of cytosolic calcium image data, *Cell Calcium* 86 (2020), 102152, <https://doi.org/10.1016/j.ceca.2019.102152>.
- I.F. Smith, I. Parker, Imaging the quantal substructure of single IP₃R channel activity during Ca²⁺ puffs in intact mammalian cells, *Proc. Natl. Acad. Sci. U. S. A.* 106 (2009) 6404–6409, <https://doi.org/10.1073/pnas.0810799106>.
- J.T. Lock, K.J. Alzayady, D.I. Yule, I. Parker, All three IP₃ receptor isoforms generate Ca²⁺ puffs that display similar characteristics, *Sci. Signal.* 11 (2018), <https://doi.org/10.1126/scisignal.aau0344> eaau0344.
- G.D. Dickinson, D. Swaminathan, I. Parker, The Probability of triggering calcium puffs is linearly related to the number of inositol trisphosphate receptors in a cluster, *Biophys. J.* 102 (2012) 1826–1836, <https://doi.org/10.1016/j.bpj.2012.03.029>.
- D.L. Prole, C.W. Taylor, Inositol 1,4,5-trisphosphate receptors and their protein partners as signalling hubs, *J. Physiol.* 594 (2016) 2849–2866, <https://doi.org/10.1113/JP271139>.
- J.T. Lock, I.F. Smith, I. Parker, Spatial-temporal patterning of Ca²⁺ signals by the subcellular distribution of IP₃ and IP₃ receptors, *Semin. Cell Dev. Biol.* 94 (2019) 3–10, <https://doi.org/10.1016/j.semcdb.2019.01.012>.
- K. Uchida, M. Nakazawa, C. Yamagishi, K. Mikoshiba, H. Yamagishi, Type 1 and 3 inositol trisphosphate receptors are required for extra-embryonic vascular development, *Dev. Biol.* 418 (2016) 89–97, <https://doi.org/10.1016/j.ydbio.2016.08.007>.
- F. Yang, L. Huang, A. Tso, H. Wang, L. Cui, L. Lin, X. Wang, M. Ren, X. Fang, J. Liu, Z. Han, J. Chen, K. Ouyang, Inositol 1,4,5-trisphosphate receptors are essential for fetal-maternal connection and embryo viability, *PLoS Genet.* 16 (2020), <https://doi.org/10.1371/journal.pgen.1008739>.
- K. Miyasaka, T. Fujimoto, T. Kawanami, S. Takiguchi, A. Jimi, A. Funakoshi, S. Shirasawa, Pancreatic hypertrophy in Ki-ras-induced actin-interacting protein gene knockout mice, *Pancreas* 40 (2011) 79–83, <https://doi.org/10.1097/MPA.0b013e3181f66c22>.